Size-Dependent Optical Properties of Polydiacetylene Nanocrystal

Victor V. Volkov,[†,§,||] Tsuyoshi Asahi,[*,†,§] Hiroshi Masuhara,[*,†] Akito Masuhara,[‡,§] Hitoshi Kasai,[‡,§] Hidetoshi Oikawa,[‡,§] and Hachiro Nakanishi[‡,§]

Department of Applied Physics, Osaka University, Suita, Osaka 565-0871, Japan, Institute of Multidisciplinary Research for Advanced Materials Science, Tohoku University, 2-1-1 Katahira Aobaku, Sendai 980-77, Japan, and CREST, JST, Kawaguchi, 332-0012, Japan

Received: December 31, 2003

We have investigated size-dependent optical properties of poly-1,6-di(*N*-carbazolyl)-2,4-hexadiyne (poly-DCHD) nanocrystals in ensemble and in a single particle level. Our experimental results demonstrate that far-field microscopy coupled with an AFM setup is a reliable experimental approach for investigating optical properties of single organic nanoparticles. Single poly-DCHD nanocrystals show resonant Rayleigh scattering spectra with a lower resonance energy peak for nanocrystals having larger cross-section against its long axis. We also examined the extinction and the resonant Rayleigh scattering spectra in ensemble and the resonant Rayleigh and Raman scattering spectra and their anisotropy of single nanocrystals. The results indicate that the size-dependent resonance peak of the polymer-backbone electronic transition can be ascribed to structural confinement of nanocrystals, which reduces the effective conjugation length of π-electron in the polymer backbone for nanocrystals with a small cross-section.

Introduction

A variety of organic nanostructures show size-dependent resonance in electronic transitions. One of the most obvious examples is poly-DCHD, which demonstrates dependence of the electronic resonance in optical extinction when the size of the material is reduced to the submicron range. Poly-DCHD has received much attention as a typical polydiacetylene (PDA). Since Wegner had shown that large single crystals of π-conjugated PDA could be obtained through solid-state polymerization of diacetylene (DA) monomer crystals,[1,2] the electronic properties of these polymers have attracted considerable attention among material scientists[3−5] and optical spectroscopists.[6−14] The π-electron conjugation along the polymer backbone guaranteed a large third-order optical nonlinearity, and thus promised this group of materials for applications to fast optoelectronics. Furthermore, the delocalization of π-electrons makes PDA a good model system for experimental and theoretical studies on electronic and structural properties in one-dimensional photoconductors. As a result, the optically allowed electronic transitions, the vibrational relaxation. and the carrier recombination pathways are well-documented for a variety of PDA. The ultrafast transient absorption experiments by Kobayashi et al. yielded a concept of localization of an optically promoted ^1B_u free exciton (FE) to a 2^1A_g state with subsequent tunneling to the ground state.[11,12,15] The time-resolved emission studies by Schott et al. revealed that at least three in-gap states could be involved in the relaxation after photoexcitation.[16] A variety of relaxation processes, implying the coexistence and the competition of singlet and triplet excitons, single and multiple polarons, has been considered to explain the experimental findings.[12,17]

The majority of reports on PDA dealt with thin polycrystalline sheets, where a fraction of PDA chains was embedded in a DA monomer crystalline environment. Recent structural studies indicated structural uncertainty in such systems. For example, it is known that poly-DCHD crystals possess a backbone of the highest degree of order and stability compared to other PDA.[18] Nevertheless, the high-resolution TEM observation on PDA structural properties in epitaxially grown thin films of DCHD monomers clearly showed a variety of coexisting monomer and polymer micro-domains formed at elevated temperature.[19] The authors reported that the needlelike micro crystals were the most obvious fully polymerized and stable structures in their films. An additional complication in PDA thin films is expected, because both the epitaxial growth of monomer sheets and the polymerization depend structurally on PDA−substrate interaction and mismatch. In an attempt to overcome structural uncertainty in PDA polycrystalline sheets, we focused on preparation of monomer and polymer nanocrystals of DCHD with narrow size and shape distributions.

Both the steady-state and the time-resolved optical studies in aqueous suspensions of poly-DCHD nanocrystals revealed a number of interesting dependencies of extinction resonance energy and recovery times on the size of the prepared nanocrystals.[20−22] Reported phenomena raised questions concerning the nature of the excited state and its relaxation dynamics in this class of materials. In this work, we will answer the question by investigating optical properties of nanocrystals in ensemble and microscopically at a single-crystal level. In the latter case we monitor the topography, the Rayleigh, and the Raman scattering responses at the same time. The Rayleigh scattering provides the direct measure of the backbone electronic properties, while the Raman spectral properties gave the better view on the structural aspects.

Experimental Section

Materials. The DCHD nanocrystals were prepared using the reprecipitation method as described elsewhere.[23,24] The poly-DCHD nanocrystals were prepared by solid-state polymerization

* Corresponding authors. E-mail (Asahi): asahi@ap.eng.osaka-u.ac.jp.
† Osaka University.
‡ Tohoku University.
§ CREST, JST.
|| Present address: Physikalisch-Chemisches Institut, Winterthurerstrasse 190, 8057, Zürich.

10.1021/jp031369o CCC: $27.50
Published on Web 05/12/2004

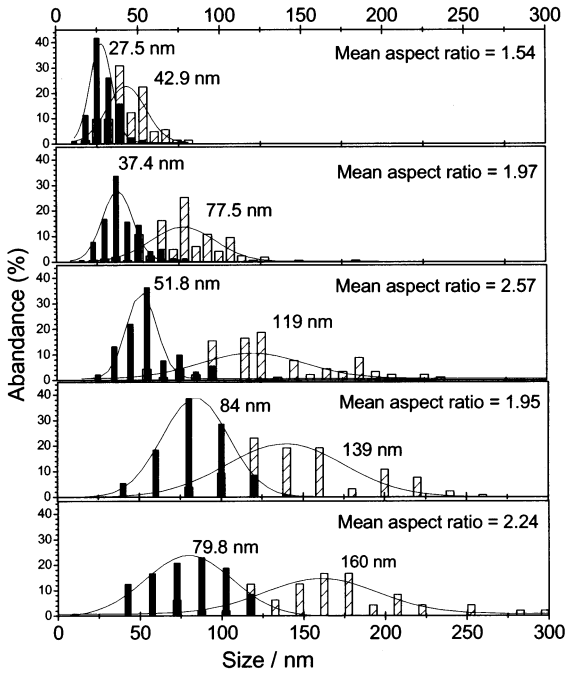

Figure 1. The size distributions for poly-DCHD nanocrystals of the prepared water dispersion samples.

in the size-controlled monomer DCHD nanocrystals dispersed in water. The size distributions for the prepared systems were estimated using images acquired with a scanning electron microscope (SEM) (Hitachi S-900).

Spectroscopy. The optical properties of poly-DCHD nanocrystals in ensemble were examined using water suspensions. The UV−Vis extinction and scattering spectra were measured using a UV−Vis−NIR scanning spectrophotometer (Shimadzu UV-3100PC) and a fluorescence spectrophotometer (Hitachi F-4500) in the synchronously scanning mode, respectively. Second, we accomplished simultaneous optical scattering microspectroscopy and topography measurements on single poly-DCHD nanocrystals using an inverted microscope (Olimpus IX70) coupled with a tapping mode AFM setup (Digital Instruments). Microscopy measurements were done for poly-DCHD nanocrystals cast on the dry PVA films. Optical Rayleigh scattering was collected in the dark-field geometry using a spectrometer (Acton Research Spectra Pro 300i) with a 150 gr/mm grating and a liquid nitrogen cooled CCD camera (Roper Scientific LN/CCD-1340/100-EB/1). A halogen lamp (Hoya Schott Megalight 100) was used as a light source.

Resonance Raman spectra were measured using a He−Ne laser at 632.8 nm and the same detection setup with a 600 gr/mm grating. In the case of ensemble measurements, the spectrum was recorded in the second order of diffraction of our grating (600 gr/mm). The single particle spectra are recorded in the first order of diffraction. This is the reason for the higher spectral resolution in Figure 6.

The anisotropy for both Rayleigh and the Raman scattering was measured by placing an analyzer after the objective lens. The simultaneous measurements of the topography and the anisotropy of the Rayleigh scattered light from an edge of a 100 nm gold film allow us to calibrate the angle of the analyzer with the respect to a physical orientation on a sample surface.

Results

Measurements in Ensemble. Figure 1 shows the size distribution of poly-DCHD nanocrystals for the prepared samples (see typical SEM images in refs 23 and 24). For each sample we determine the mean aspect ratio, which is the ratio between the most abundant length and width values estimated statistically. The mean ratio increases in the series of systems where the long axis increases from 40 to 100 nm. However, the mean aspect ratio decreases again for the nanocrystal with the long axis in the range of 100 to 160 nm. The statistical evaluations show that the systems with the dominant axis of 140−160 nm demonstrate a higher content of rodlike and nearly cubic forms where the short axis is up to 130 nm (also see refs 23 and 24). In the fibrous crystals of 0.7 to 9 μm, the short axis is in the range of 30 to 70 nm, which is essentially smaller if compared to that in the rodlike nanocrystals of 100 to 160 nm.

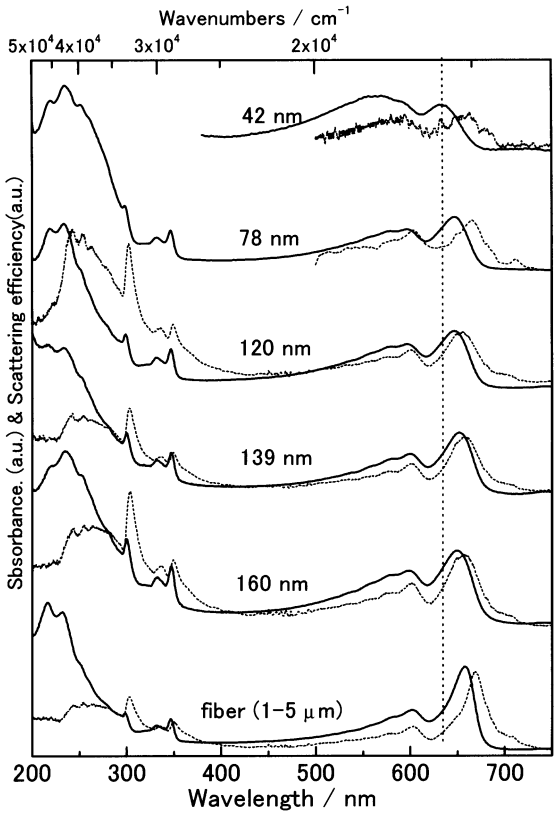

Figure 2. The extinction (solid line) and the scattering (dashed line) spectra of poly-DCHD nanocrystals in suspensions in dependence on the statistically estimated mean long axis values.

Figure 2 shows both the optical extinction and scattering spectra of poly-DCHD nanocrystals in the UV to near-IR spectral range, depending on their size. The lower-energy part of the optical extinction consists of two spectral features: the resonance with the $\pi-\pi^*$ electronic transition to the first allowed excited state in the range of 630 to 660 nm (1.58×10^4 to 1.53×10^4 cm^{-1}) and the blue side series of weaker transitions due to the vibronic progression of C=C stretching as discussed in the literature.[11,25] Furthermore, in this manuscript, we will name the main peak and the vibronic feature in this transition to the first excited state of the backbone as (0−0′) and (0−n′), respectively. The near UV part of the extinction (scattering) spectra indicates a pair of narrow resonances at 350 nm (2.86×10^4 cm^{-1}) and 300 nm (3.33×10^4 cm^{-1}) due to the carbazolyl electronic transitions to the first and second excited states, respectively.[18]

Figure 3 represents the carbazolyl optical extinction spectra in 120 nm DCHD crystals before and after polymerization. The optical extinction spectra reveal that both carbazolyl electronic transitions are associated with the vibrational progression on

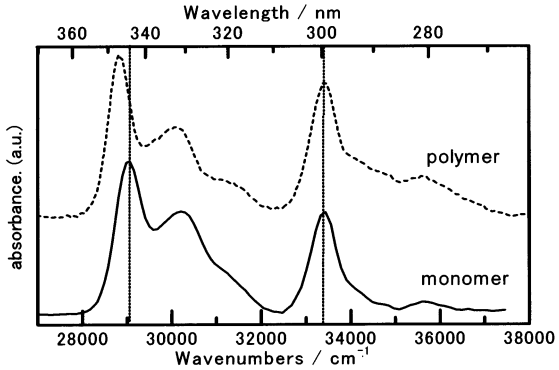

Figure 3. The extinction spectra of carbazolyl electronic transitions in DCHD nanocrystals with a mean size of 120 nm before (solid line) and after polymerization (dashed line).

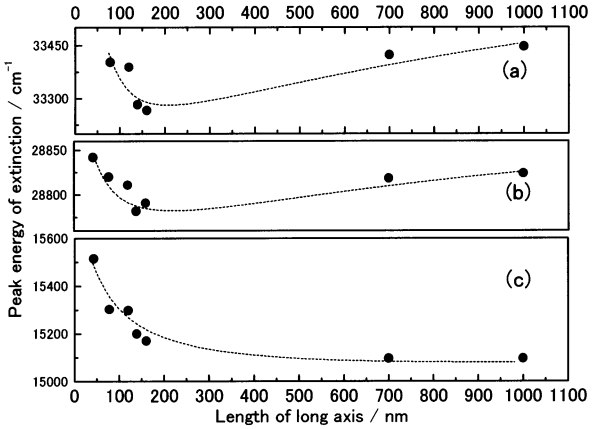

Figure 4. The peak energy of the backbone and the carbazolyl electronic transition bands in the extinction spectra of the suspensions of poly-DCHD nanocrystals as a function of their mean length.

frequencies of C−C in-plane and C−H in-plane stretching modes and ring deformations. The carbazolyl electronic transition to the second excited state does not change upon polymerization, while the transition to the first excited state shifts to a lower energy. This could be due to the fact that its dipole moment of the second excited state is nearly perpendicular to that along the polymer backbone.[3]

In Figure 4 we show the peak energy of backbone and carbazolyl bands in the optical extinction spectra as a function of the nanocrystal length estimated statistically. One can clearly see the "optimization" of the energy for the electronic transitions when the nanocrystal long-axis increases from 40 to 150 nm. However, in contrast to the lowest energy of the backbone electronic transition, the peaks of carbazolyl transitions increase in energy in the fibrous systems. This observation certainly has attracted our attention. Recent results on high-resolution transmission electron microscopy indicate that the backbone chains in an elongated nanocrystal lie parallel with respect to the long axis of the nanocrystal.[26] The crystallographic data on this matter[3] thus indicate that the carbazolyl groups in a DCHD crystal are oriented in the dimension of the short axis of the crystal. The statistics of nanocrystal size and shape in Figure 2 shows that the systems with the dominant axis of 140−160 nm demonstrate higher content of cubic and nearly cubic with a large cross-section. The same statistics also indicate that the short axis decreases in the fibrous systems. Therefore we consider that the observed electronic properties of carbazolyl in poly-DCHD nanocrystals reflect the degree of structural compaction in the direction of the short axis in poly-DCHD nanocrystals.

The backbone optical extinction shifts to lower energy upon size increment as shown in Figure 4. In the ensembles of nanocrystals larger than 160 nm, the backbone optical extinction resonance reaches the saturation at the energy similar to that in a poly-DCHD bulk crystal. This is consistent with the previously reported data.[20−22] It should be, however, noted that the optical extinction is a sum of optical absorption Q_{abs} and scattering Q_{sct} coefficients. In dipole moment approximation, the optical extinction of a small spherical particle with a diameter d can be expressed as[27]

$$\alpha_{ext} = N\pi\left(\frac{d}{2}\right)^2(Q_{abs} + Q_{sct}) = N\pi\left(\frac{d}{2}\right)^2\left(4x\,\mathrm{Im}\left\{\frac{\epsilon_1 - \epsilon_m}{\epsilon_1 + 2\epsilon_m}\right\} + \frac{8}{3}x^4\left|\frac{\epsilon_1 - \epsilon_m}{\epsilon_1 + 2\epsilon_m}\right|^2\right) \quad (1)$$

where N is the number of particles per unit of volume, n is the reflective index of the surrounding media, λ is the wavelength of light, x is the size factor defined by $\pi nd/\lambda$, and ϵ_1 and ϵ_m are the permittivities of the particle and the surrounding medium, respectively.

The scattering spectra from each poly-DCHD system are red-shifted compared to the extinction spectra as shown in Figure 2. Even though the Kramars-Kronig transform relates both the imaginary and the real parts of permittivity, the absorption and scattering spectra have different content. The scattering response according to the eq 1 is a combination of relative permittivity components where the real part contributes to a low-energy shift of the scattering resonance compared to the absorption and extinction. Also, eq 1 indicates that the absorption contribution proportional to d^3 while the scattering one is to d^6, which means these contributions in the extinction spectrum is a function of the particles size, too. As a result, one may consider that the size dependence of the poly-DCHD backbone extinction (Figure 4) may represent the increase of the scattering contribution for larger nanocrystals. However, our measurements in suspensions and single-particle spectroscopy investigations in polymer films[28] demonstrate that the scattering spectra also show a size-dependent variance.

The results of the measurements in aqueous suspensions of poly-DCHD nanocrystals revealed several problematic issues we have to consider further. First, both the extinction and the scattering spectra indicate that the relative permittivity of poly-DCHD nanocrystals is a size/shape-dependent function. Second, the carbazolyl electronic properties may provide a good diagnostics to local structural environment. Third, SEM observation and its statistics[23,24] indicated that the prepared ensembles possess a degree of structural and dimensional heterogeneity. Thus optical extinction measurements in a water suspension of poly-DCHD nanoparticles would include an ambiguous correlation between electronic properties of poly-DCHD and statistically estimated size parameters. Therefore, we further provide and discuss our results of light scattering microspectroscopy in a single nanocrystal level.

Single-Particle Microspectroscopy. The application of far-field microscopy coupled with a tapping mode AFM setup allowed us to observe the topography of a nanostructure and its optical response at the same time. Using the AFM observation, we may summarize here that poly-DCHD nanocrystals can pack in three types of structures: small sphere-like, rodlike, and fiber-like nanocrystals. Figure 5 demonstrates both topography and scattering spectra for the selected single poly-DCHD nanocrystals. The shape of the scattering spectra is simpler compared to that recorded in extinction. In most cases, we were

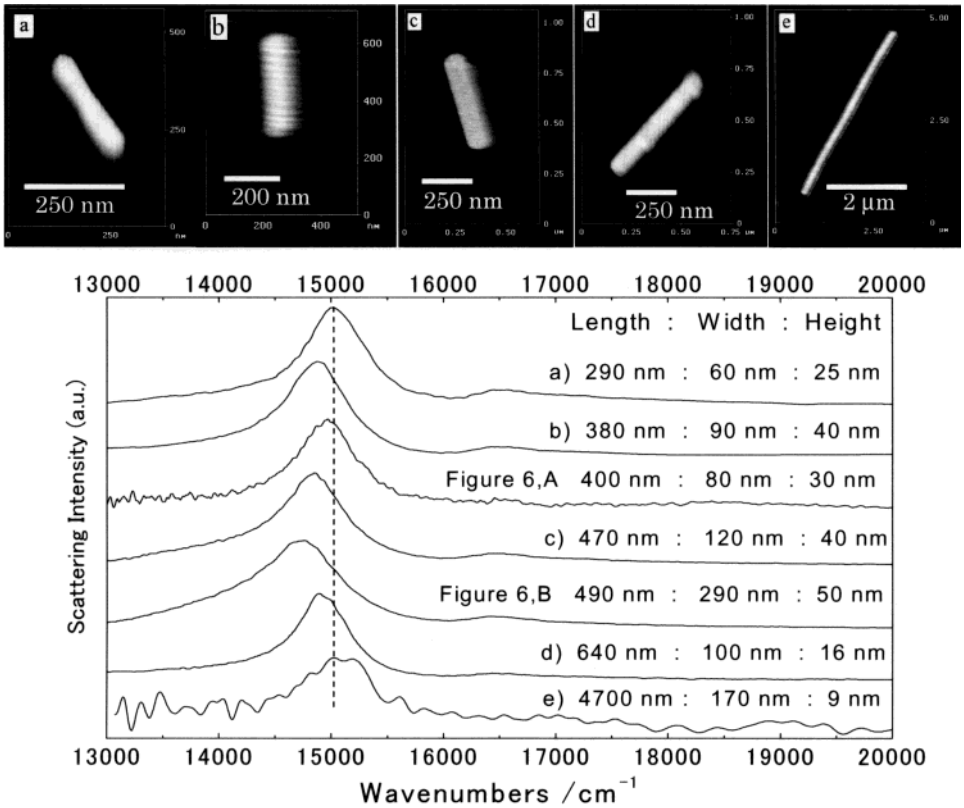

Figure 5. AFM topographic images for the selected poly-DCHD nanocrystals and their Rayleigh scattering spectra. The estimated length, width, and height for these nanocrystals are provided next to each spectrum.

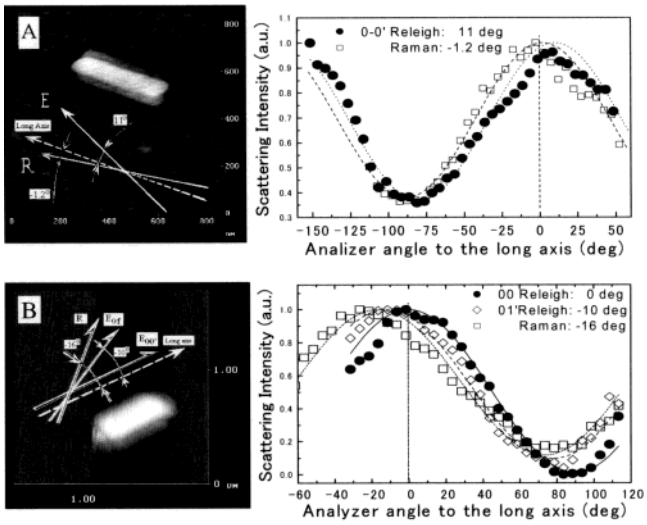

Figure 6. AFM topographic images of two poly-DCHD nanocrystals and the anisotropy for the Rayleigh scattering and the Raman scattering of the C═C stretching modes with respect to the long axis of each nanocrystal.

able to de-convolve it using a sum of Lorentzian functions. As in the case of extinction response, the optical scattering shows two spectral features. The first one is the dominant band of the $0-0'$ electronic transition at 1.50×10^4 cm^{-1} with a fwhm of about 600 cm^{-1}. The second feature is the weak $0-n'$ peak of the vibronic progression on the first excited state. The energy difference between the two peaks is about 1500 cm^{-1}, which corresponds to the C═C stretch (1460 cm^{-1}) that we monitored in resonance Raman scattering (see Figure 6). Figure 5 clearly demonstrates that the maximum of the electronic resonance energy does not follow any obvious dependence on the long-axis length of the crystals. Higher energy response is observed both in the smaller and in the fibrous-like systems. The lowest-energy electronic resonance is realized in the systems where the width and the height are larger, as will be discussed later.

The electronic resonance for the Rayleigh scattering did not show any difference in energy when detected under different angles of the analyzer, while its anisotropy demonstrates a relatively high contrast. This is because the dielectric tensor component along the PDA backbone is the only contribution in optical properties in the visible, which supports the view on PDA systems as one-dimensional π-conjugation systems. The ratio of intensities for the $0-0'$ and the $0-n'$ spectral components slightly decreases only when the analyzer is near the cross geometry with the long axis. Spectral deconvolution yielded the anisotropies for both $0-0'$ and $0-n'$ spectral components with respect to the topographies of the single nanocrystals. The results are shown in Figure 6. For the case of a nanocrystal, the orientation of the $0-0'$ in Rayleigh scattering may not be parallel to the long axis of the nanocrystals (case B in Figure 6). However, following the same approach we observe it to be parallel to the long axis in fibrous nanocrystals, which is consistent with the results of high-resolution TEM studies.[26] Under the same experimental conditions to the Rayleigh scattering response, we estimated the anisotropy of the Raman scattering for both C═C and C≡C stretching modes also. The results indicate that the stretching modes in the ground state are about 12°−16° off the electronic transition dipole moment. The anisotropy of the Rayleigh $0-n'$ spectral component is proximal to that in the resonant Raman case, as the momentum vector $h\Omega$ of the backbone stretching vibrations in the excited state at 1500 cm^{-1} (contribution to the $0-n'$ scattered component) obeys the vector relation $h\mathbf{k}_{0-n'} = h\mathbf{k}_{0-0'} + h\Omega_n$.

Figure 8 correlates energy of the backbone resonance maximum with the length and the topological cross-section of

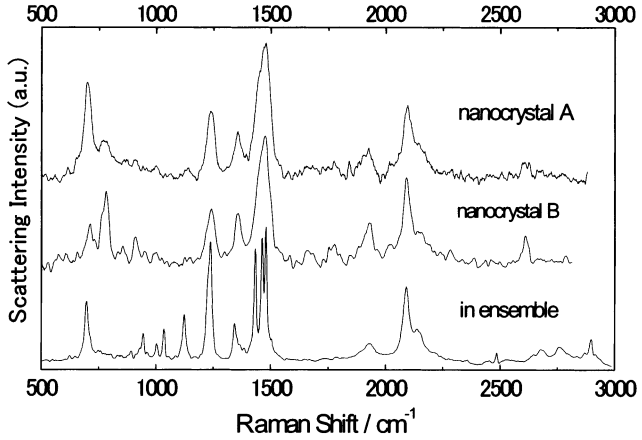

Figure 7. Resonant Raman spectra from the single poly-DCHD nanocrystals A (top) and B (middle) in Figure 6, and corrected in ensemble.

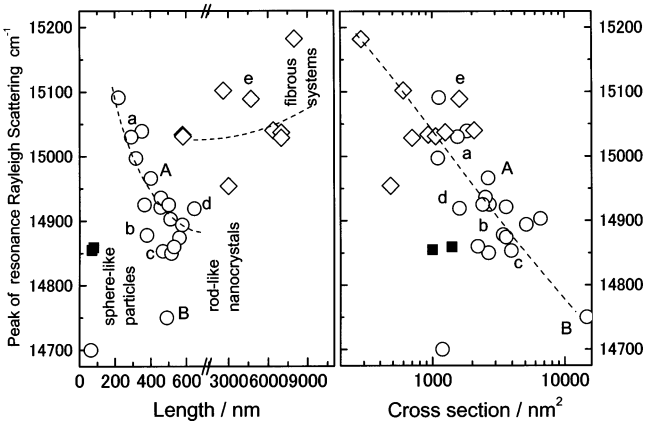

Figure 8. Dependence of backbone optical resonance on length and cross-section. Solid squares, open circles, and open diamonds represent results for sphere-like, rodlike, and fibrous-like nanocrystals respectively. The letters marking indicate the data for the nanocrystals shown in Figures 5 and 6.

nanocrystals. The dependence on the length (the left part in Figure 8) indicates that the sphere-like, the rodlike, and the fiberlike nanocrystals have different electronic properties. In the case of the rodlike nanocrystals, the backbone resonance is lower in energy for the longer systems. In the fibrous nanocrystals (typically longer than 600 nm), the scattering response shifts to a higher energy region. We do not yet have any consistent and sufficient data for the small systems to make certain conclusions on their electronic properties. Tentatively, a small sphere-like system shows a low-energy and broad (fwhm of 1000 cm^{-1}) electronic resonance when detected in the scattering. The shape dependence of electronic response in single-particle scattering acquires a clear presentation, when expressed with respect to the topographical cross-section of the nanocrystals, see the right part in Figure 8. Specifically, our results of the optical scattering studies on a single-particle level reveal a linear relation of the backbone electronic resonance on the logarithm of the cross-section of nanocrystals, and the crystals with the smaller cross-section possess the backbones with the electronic response at higher energy.

Discussion

The steady-state optical studies in aqueous suspensions of poly-DCHD nanocrystals revealed the dependencies of the ground-state extinction resonance energy on the mean length of prepared nanostructures. Now we explain this phenomenon considering the quantum confinement effect, Mie scattering factor, π-electron effective overlap, and structural confinement. In the case of poly-DCHD, however, the dielectric screening is small,[11] so that the relatively small Bohr exciton radius in poly-DCHD allows us to disregard the possibility of the quantum confinement effect discussed in inorganic semiconductor systems.

The size of our poly-DCHD nanocrystals is in the order of hundreds of nanometers, which is comparable to the wavelength of visible light. In such case, the so-called Rayleigh approximation, eq 1, does not hold for the optical response from such particles in general. We have to consider the Mie scattering or the microcavity effect. This is the case when both the absorption and the scattering responses are the functions of size and shape. These functions could yield a size (shape)-dependent optical response of poly-DCHD, even if the permittivity of poly-DCHD nanocrystals is independent of size. Because the Rayleigh scattering anisotropy (Figure 6) demonstrates that the major component of the dielectric tensor of the nanocrystals lies nearly along the long axis of a nanocrystal, one can expect that the microcavity effect will change the resonance peak as a function of the nanocrystals length. However, Figures 5 and 8 indicate that the backbone electronic resonance does not show any dependence on length. Additionally, we examined the refractive index effect of the surrounding media on the resonance peak of the extinction of the suspension changing the solvent from pure water to aqueous solutions of ethylene glycol, DMSO, and pyridine. However, we did not observe any systematic dependence on the refractive index as expected from the Mie scattering theory. Consequently, it can be concluded at the present stage of the investigation that the Mie scattering factor is negligible or not dominant in the size-dependent backbone resonance of poly-DCHD nanocrystal.

A very attractive approach in explanation of the size-dependent optical properties in organic materials is due to the effective conjugated length of the π-electron. It brings into attention structural properties of prepared systems, because the length of the backbone planar segment determines the extension of the π-electron in the backbone, and consequently the electronic band-gap.[29] Therefore, the higher concentration of structural defects (sp^3 states, kinks, twist around C−C bond, dislocations) would reduce the effective conjugation length and contribute to a blue shift in the electronic transition peak. Early investigations of the optical properties of PDA systems in solutions and films demonstrated the reciprocal character of the relation between the conjugated length and the resonance energies in its optical response. Chance et al. considered that the electronic transition energies and the C═C stretching band could give the phenomenological estimation of the number of the repeating units involved in π-electron delocalization.[30]

Following the conjugation length approach, we rationalize the results on the optical extinction in ensembles of poly-DCHD nanocrystals as a direct indication of better backbone planarity in the longer systems, including the fibrous crystals. Unfortunately, this is in controversy with the results of our studies on backbone Rayleigh scattering in single nanocrystals. Also it is inconsistent with the experimental findings in resonance Raman experiment on C═C and C≡C stretching mode frequencies (both in ensembles and in single crystals). The Raman peak shows a better π-electron overlap in the polymer backbone when the mean length of the nanocrystals increases up to 300 nm only. Both Raman stretching modes shift to higher frequencies for the systems longer than 500 nm. Interestingly, the character of the dependence of C═C and C≡C stretching frequencies on

the length is similar to that for backbone Rayleigh scattering in single nanocrystals and to that the carbazolyl electronic transitions detected in ensembles (Figure 4).

It is important to consider why the backbone optical extinction in the ensembles of fibrous nanocrystals is not consistent with all other data represented in this work. Our AFM studies reveal that a sample of the fibrous system is structurally heterogeneous. Specifically it typically contains a population of small nanocrystals (about 70−100 nm). Also, our single-particle spectroscopy coupled with AFM observation of the sample is limited for several thin fibrous crystals. On the other hand, the rodlike nanocrystals in the range of 150 to 500 nm show a higher degree of structural homogeneity, which possibly makes their extinction response in ensemble and their scattering response on a single-particle level consistent with each other. Besides the structural heterogeneity, we observed the presence of aggregates and assemblies in all samples. Therefore, we may count the inconsistency of the extinction response with the other experimental findings to the complex nature of the extinction function, which is the sum of scattering and absorption contributions of all possible structural species in a suspension.

The main result of our experimental efforts in a single nanocrystal level is the linear relation between the backbone electronic resonance and the logarithm of the cross-section of nanocrystals. Taking into account the findings of the Raman experiment, we can state generally that poly-DCHD possesses shorter conjugated length in the nanostructures with a smaller cross-section. Moreover, considering the general knowledge of the poly-DCHD structure[3] and the backbone orientation with respect to the nanocrystals topography (see Figure 6), we find that the bulky and rigid character of the side group is the dominant contribution to the decrease of the effective conjugation length in the nanocrystals with a smaller cross-section. Two decades ago, Chance et al. used the semiempirical valence effective Hamiltonian approach to anticipate the side-group strain contribution to the increase of the band-gap energy.[31] Later, the blue shift of the backbone electronic transition due to the shortening of the conjugation length was observed for a water-soluble conjugated polydiacetylene, when the disruption of the constructive hydrogen bond net caused the structural misalignment of its ionic side groups.[32] Recently, Evans et al.[33] reported on the conjugation length change in PDA Longmuir-Blodgett films upon UV-induced modification of the side group.

We prepared poly-DCHD nanocrystals here by photopolymerization of the DCHD monomer crystals obtained by the reprecipitation method. Upon photopolymerization, both the formed polymer backbone and the side groups have to find optimal structural conditions within the boundary established during reprecipitation. Such reconstruction may not always lead to a stable compromise with the boundaries at which the molecules are restricted. If such is the case, the structural strain brings the system to a cleavage on adjoined or separated segments. Monomer crystals with a larger cross-section will provide "better opportunities" for structural and electronic optimization of poly-DCHD nanocrystals. Therefore, the structural confinement in the planar direction of the cross section is the governing factor of the electronic optical properties of poly-DCHD in nanofabricates, as it leads to the carbazolyl group distortion and thus to the backbone strain. The valence effective Hamiltonian calculations predicted a stronger localization of charges on the triple bond in a strained system (with wider electronic band-gap) when compared to the electronic state in a fully optimized PDA system.[31] Figure 9 demonstrates the ratio of the Raman stretching intensity of C≡C mode to that of C═C one as a function of the electronic resonance obtained in the single nanocrystal experiments. The relation should indicate a stronger localization of π-electron on the triple bond for the nanocrystals with the higher energy electronic response.

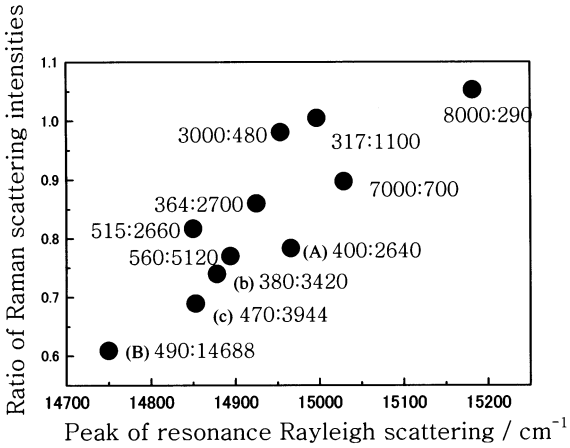

Figure 9. The intensity ratio of C≡C and the C═C stretching modes as a function of backbone electronic resonance. Each data point represents results for a single nanocrystal. The two numbers next to each point indicate the length and the cross-section in nanometers for the nanocrystals under investigation. Capital and regular letters indicate the data for the systems, topographies of which are shown in Figures 5 and 6.

Acknowledgment. The present work was supported by a grant from the Core Research for Evolution Science and Technology (CREST) of Japan Science and Technology Agent (JST).

References and Notes

(1) Wegner, G. *Z. Naturforsch. Teil. B* **1969**, *24*, 824.
(2) Wegner, G. *Makromol. Chem.* **1972**, *154*, 35.
(3) Apgar, P. A.; Yee, K. C. *Acta Crystallogr. B* **1978**, *34*, 957.
(4) Kobayashi, A.; Kobayashi, H.; Tokura, Y.; Kanetake, T.; Koda, T. *J. Chem. Phys.* **1987**, *87*, 4962.
(5) Liao, J.; Martin, D. *Science* **1993**, *260*, 1489.
(6) Sauteret, C.; Hermann, J.; Frey, R.; Pradere, F.; Ducuing, J.; Baughman, R. H.; Muller, H.; Chance, R. R. *Phys. Rev. Lett.* **1976**, *36*, 956.
(7) Chance, R. R.; Patel, G. N.; Witt, J. D. *J. Chem. Phys.* **1979**, *71*, 206.
(8) Batchelder, D. N.; Bloor, D. *J. Phys. C* **1982**, *15*, 3005.
(9) Kanetake, T.; Tokura, Y.; Koda, T.; Kotaka, T.; Ohnuma, H. *J. Phys. Soc. Jpn.* **1985**, *54*, 4014.
(10) Materny, A.; Kiefer, W.; Schwoerer, M. *J. Chem. Phys.* **1992**, *97*, 2237−2246.
(11) Horvath, A.; Weiser, G.; Lapersonne-Meyer, C.; Schott, M.; Spagnoli, S. *Phys. Rev. B* **1996**, *53*, 13507
(12) Kobayashi, T.; Yasuda, M.; Okada, S.; Matsuda, H.; Nakanishi, H. *Chem. Phys. Lett.* **1997**, *267*, 472.
(13) Haacke, S.; Berrehar, J.; Lapersonne-Meyer, C.; Schott, M. *Chem. Phys. Lett.* **1999**, *308*, 363.
(14) Chen, T.; Vierheilig, A.; Waltner, P. Heid, M.; Kiefer, W.; Materny, A. *Chem. Phys. Lett.* **2000**, *326*, 375.
(15) Kobayashi, T.; Yoshizawa, M.; Stamm, U.; Taiji, M.; Hasegawa, M. *J. Opt. Soc. Am. B* **1990**, *7*, 1558.
(16) Kraabel, B.; Joffre, M.; Lapersonne-Meyer, C.; Schott, M. *Phys. Rev. B* **1998**, *58*, 15777.
(17) Yoshizawa, M.; Taiji, M.; Kobayashi, T. *IEEE J. Q. El.* **1989**, *25*, 2532.
(18) Morrow, M. E.; Eckhardt, C. J. *Chem. Phys. Lett.* **1988**, *144*, 65.
(19) Kawase, N.; Isoda, S.; Kurata, H.; Murata, Y.; Takeda, K.; Kobayashi, T. *Polymer* **1998**, *39*, 591.
(20) Asahi, T.; Kibisako, K.; Masuhara, H.; Kasai, H.; Katagi, H.; Oikawa, H.; Nakanishi, H. *Mol. Cryst. Liq. Cryst.* **1998**, *314*, 95−100.
(21) Oikawa, H.; Oshikiri, T.; Kasai, H.; Okada, S.; Tripathy, S. K.; Nakanishi, H. *Polym. Adv. Technol.* **2000**, *11*, 783.

(22) Kasai, H.; Oikawa, H.; Nakanishi, H. In *Organic Mesoscopic Chemistry*, *Chemistry for the 21st Century*; Masuhara, H., DeSchryver, F. C., Eds.; Blackwell Science: Oxford, 2000; pp 145−170.
(23) Katagi, H.; Kasai, H.; Okada, S.; Oikawa, H.; Komatsu, K.; Matsuda, H.; Liu, Z.; Nakanishi, H. *Jpn. J. Appl. Phys.* **1996**, *35*, L1364.
(24) Matsuda, H.; Yamada, S.; Van Keuren, E.; Katagi, H.; Kasai, H.; Okada, S.; Oikawa, H.; Nakanishi, H.; Smith, E. C.; Kar, A. K.; Wherrett, B. S. *SPIE Proceedings* **1995**, *2998*, 241.
(25) Materny, A.; Kiefer, W. *Phys. Rev. B* **1992**, *46*, 2704.
(26) Kübel, C.; Martin, D. C. *Philosophical Magazine A* **2001**, *81*, 1651.
(27) Bohren, C.; Huffman, D. *Absorption and Scattering of Light by Small Particles*; John Wiley & Sons: New York, 1998.
(28) Asahi, T.; Masuhara, H. In *Single Organic Nanoparticles*; Masuhara, H., Nakanishi, H., Sasaki, K., Eds.; Springer: Berlin, Tokyo, 2003; pp 94−108.
(29) Brivio, G. P.; Milazzi, E. *Chem. Phys. Lett*. **1983**, *95*, 555.
(30) Shand, M. L.; Chance, R. R.; LePostollec, M.; Schott, M. *Phys. Rev. B* **1982**, *25*, 4431.
(31) Eckhardt, A.; Boudreaux, D. S.; Chance, R. R. *J. Chem. Phys.* **1986**, *85*, 4116.
(32) Millen, R. P.; Temperini, M. L. A.; de Faria, D. L. A.; Batchelder, D. N. *J. Raman Spectrosc.* **1999**, *30*, 1027.
(33) Cai, M.; Mowery, M. D.; Menzel, H.; Evans, C. E. *Langmuir* **1999**, *15*, 1215.